Hindawi
Mathematical Problems in Engineering
Volume 2020, Article ID 5025438, 11 pages
https://doi.org/10.1155/2020/5025438

Research Article

Analytical Method for Evaluating the Impact Response of Stiffeners in a Ship Side Shell Subjected to Bulbous Bow Collision

Min Zhang,[1,2] Zhijie Zhu,[2] Yang Zeng,[2] Jingxi Liu,[2,3] and Zhiqiang Hu[4]

[1]*School of Mechanical Engineering, Wuhan Polytechnic University, Wuhan 430048, China*
[2]*School of Naval Architecture and Ocean Engineering, Huazhong University of Science and Technology, Wuhan 430074, China*
[3]*Collaborative Innovation Center for Advanced Ship and Deep-Sea Exploration (CISSE), Shanghai 200240, China*
[4]*School of Engineering, Newcastle University, Newcastle upon Tyne, NE1 7RU, UK*

Correspondence should be addressed to Zhijie Zhu; 469087247@qq.com

Received 23 November 2019; Revised 13 March 2020; Accepted 23 March 2020; Published 14 April 2020

Academic Editor: Ali Ramazani

This paper addresses a simplified analytical method for evaluating the impact responses of the stiffeners in a ship side shell subjected to head-on collision by a bulbous bow. The stiffeners are classified as the "central stiffener" and the "lateral stiffener" according to their relative position to the bulbous bow. In analytical predictions, it is assumed that the flexural bending of the central stiffener and plate occurs simultaneously. However, the deformation mode of the central stiffener outside the indenter contact region is simplified as linear to derive its deformation resistance. The curved deformation mode of the lateral stiffener is proposed to calculate the deformation resistance and to consider the interaction effect with the plate, which can cause the plate to fracture earlier. Model tests with three specimens (one unstiffened plate for reference and two stiffened plates) quasistatically punched by a conical indenter are performed to validate the proposed analytical method. Resistance-penetration curves and damage shapes for the three specimens are obtained. The experimental results illustrate the effects of the stiffeners on the deformation resistance and fracture initiation of the stiffened plate and the influence of stiffener tripping on the lateral resistance. Moreover, the experimental and analytical predicted results correspond well, suggesting that the proposed analytical method can accurately predict the crashworthiness of a ship side shell subjected to bulbous bow collision.

1. Introduction

Ship side shells are generally equipped with stiffened steel panels to simplify fabrication; additionally, these panels have an excellent strength-to-weight ratio. During the sailing life of a ship, the ship side may suffer various types of loads. Among the applied loadings, the load from a collision with another ship can lead to serious consequences, such as loss of structural integrity, flooding of the ship tank, and severe oil pollution. Therefore, accurate crashworthiness assessment of ship side shells in the predesign stage has been continuously studied by engineers.

The commonly used approaches in ship collision investigations are experiments, numerical simulations, and simplified analytical methods [1]. Experiments can provide reliable data with respect to deformation and failure patterns and the characteristics of resistance-penetration responses, which can be used to verify the other two methods. A number of scaled model tests of stiffened plates punched by a spherical or conical indenter to fracture initiation have been performed [2–5]. In all the tests, the stiffeners can be generally categorized into two types due to the different deformation driving factors. Taking the experiments conducted by Kõrgesaar et al. [4] as an example, as shown in Figure 1, the stiffener immediately below the indenter, the "central stiffener," deforms due to the direct punch of the indenter. The deformation of the stiffener away from the impact position, the "lateral stiffener," is driven by the deformed plate. In previous model tests, the deformation patterns of the lateral stiffener were similar. For the central stiffener, different tripping extents can be observed.

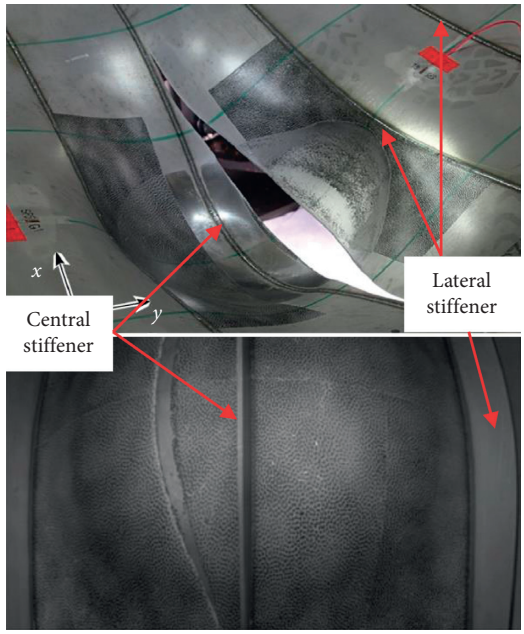

Figure 1: Different types of stiffener [4].

Therefore, the influence of central stiffener tripping on the lateral deformation resistance is particularly investigated through model tests.

Unlike experiments, numerical simulations are low-cost and easily repeatable with the help of powerful computers. The numerical simulation method has the ability to predict the collapse mode and reaction force of structures subjected to collisions when provided with appropriate modeling parameters. Until now, numerous failure criteria considering different factors (stress state, loading path, mesh size, strain rate, etc.) that can influence plate fracture have been proposed to predict the initial fracture of ship structures in collision and grounding analysis [6–8].

Compared with the first two methods, the simplified analytical method is the preferred tool in the predesign stage because this method can most rapidly assess the crashworthiness of ship structures [9–11]. Extensive studies have been conducted to estimate the large deformation resistance and fracture initiation of an unstiffened plate subjected to lateral indentation by a spherical indenter [12–15]. Analytical methods for the stiffener components of the stiffened plate were generally proposed in cases in which the stiffened plates were punched by indenters with linear or rectangular tops [16–19]. In these studies, both the deformation modes of the plate and the attached stiffeners are treated as a linear form, where the lateral resistances of the stiffeners are attributed to the rotation of the plastic hinges at the applied load and the support and membrane tension over the plastically deformed region. However, the deformation modes of the stiffeners are different in the cases of a stiffened plate punched by a sphere. As shown in Figure 1, the deformation mode of the central stiffener is consistent with that of the plate, i.e., with a curved deformation profile and a spherical top. In addition, the deformation mode of the lateral stiffener is identical to that of the deformed plate, i.e., with a curved deformation profile. Until now, analytical methods to obtain the lateral indentation resistances for these two different forms of stiffeners have seldom been referred to. Therefore, the current study is intended to present the deformation modes of the central and lateral stiffeners and the corresponding deformation resistances.

Moreover, fracture prediction of the ship side plate is crucial for estimating energy dissipation and structural resistance. Several analytical expressions have been proposed to obtain the critical penetration depth of an unstiffened plate indented by a sphere [12–15]. Nevertheless, the added stiffeners can lead to higher stiffness but reduce flexibility and result in earlier fracture compared with the response of an unstiffened plate [2]. Therefore, an analytical solution for the influence of stiffeners on the critical penetration depth of the plate should be investigated. In summary, the aim of the present analytical study is to build equations to predict the deformation resistances of the attached stiffeners in the stiffened plate and the initial fracture of the stiffened plate.

In this study, simplified analytical methods are proposed to predict the deformation resistance and the critical penetration depth of a stiffened plate punched by a bulbous bow. Deformation modes for the central and lateral stiffeners are proposed, and the resistance-penetration relations are derived by theoretical calculations. In addition, the reduction in the critical penetration depth with the stiffener is derived considering the interaction effect between the plate and the stiffener. Moreover, experimental tests are conducted on specimens with different numbers of stiffeners quasistatically punched by a conical indenter. The experimental results validate the feasibility of the proposed method. Finally, some conclusions are drawn.

2. Analytical Predictions

This section presents analytical predictions for the large deformation resistances of the central and lateral stiffeners and the initial fracture of the stiffened plate in a typical ship bulbous bow-side collision scenario, as shown in Figure 2. In developing the analytical solutions, several assumptions are made as follows:

(1) The ship side shell is assumed to undergo head-on collision by a bulbous bow at the midspan between the web girders.

(2) The web girders are assumed to be stiff enough to constrain the boundary of the outer side plate.

(3) The bulbous bow is assumed to be rigid, and the shape of the bulbous bow is simplified as conical.

(4) The residual stress and initial deflection of the stiffened plate are not considered.

Based on the assumptions, theoretical deformation modes and the derived formulae for the central stiffener and the lateral stiffener are described in detail. The deformation shape of the central stiffener is identical to that of the plate, but the region not in contact with the indenter is treated as linear to merely calculate the lateral resistance for simplicity. In particular, a curved deformation mode for the lateral stiffener is proposed to consider its interaction effect with

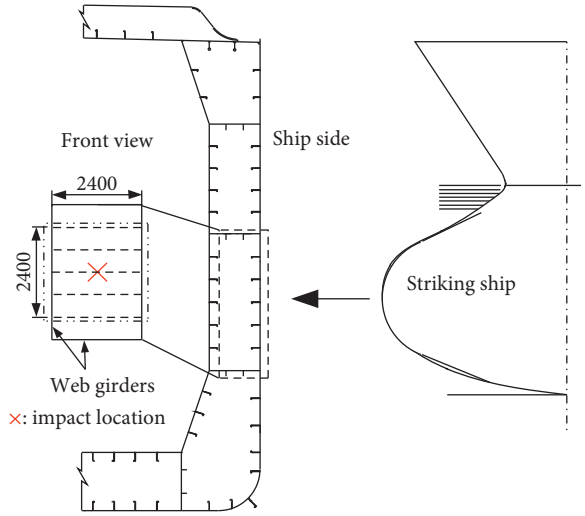

Figure 2: Ship bow-side collision scenario.

the side plate, which can influence the initial fracture of the ship side plate.

2.1. Large Deformation Resistance of the Stiffeners. The analytical method to predict the deformation resistances of the central and lateral stiffeners is presented in this section. In general, the stiffener used for ship construction is the bulb-bar stiffener. Nevertheless, the resistance of the flat-bar stiffener is analyzed for simplicity.

2.1.1. Central Stiffener. The movement of the central stiffener is driven by the indenter; thus, the deformation shape of the central stiffener is the same as that of the side plate. In the whole deformation process, the central stiffener is assumed to maintain an in-plane deformation process, i.e., tripping of the stiffener is ignored.

Initially, in the elastic stage, the central stiffener mainly exhibits a bending effect. Assuming that the central stiffener is placed in the x-w coordinate system, as shown in Figure 3, the external load work is equal to the strain energy:

$$\frac{F_{e\_cs} w_{csmax}}{2} = \int_{lcs} \frac{M_{e\_cs}^2(x)}{2EI_{cs}} dx, \tag{1}$$

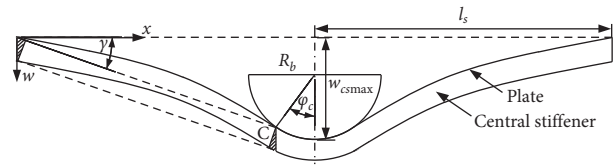

Figure 3: Deformation mode of the central stiffener.

where w_{csmax} is the maximum deflection of the central stiffener, l_{cs} is the length of the central stiffener, F_{e_cs} is the external load at the elastic stage, $M_{e\_cs}(x)$ is the moment in the stiffener applied by F_{e_cs} and can be obtained as $M_{e\_cs} = F_{e\_cs}x/2$, E is the elastic modulus, and I_{cs} is the moment of inertia. In the pure bending state, the neutral axis for the stiffened panel is located in the plate, and the stiffener dominates the bending effect [20]. I_{cs} can be expressed as

$$I_{cs} = \frac{h_s^3 t_s}{3}, \tag{2}$$

where h_s and t_s are the height and thickness of the stiffener, respectively.

Then, according to the energy method, the instantaneous force of the stiffener in the elastic stage can be obtained by integrating equations (1) and (2):

$$F_{e\_cs} = \frac{2Eh_s^3 t_s w_{csmax}}{l_s^3}, \tag{3}$$

where l_s is the half-length of the stiffener.

In the plastic stage, the stiffener will experience bending and tension simultaneously. This deformation mode is also shown in Figure 3. According to Zhang et al. [15], the deformation shape of the curved stiffener can be expressed by a parabola:

$$x(w) = \frac{w^2 - 2w_{csmax} w}{2R_b(\cos\varphi_c - 1)\tan\varphi_c}, \tag{4}$$

where x and w are the horizontal and vertical distances from any point on the plate to the plate boundary, R_b is the radius of the sphere, and φ_c is the angle from the center of the indenter to point C, as shown in Figure 3. Point C is the outmost contact point between the plate and the indenter.

Moreover, w_{csmax} can be expressed as

$$w_{csmax}(\varphi_c) = \sqrt{2(l_s - R_b \sin\varphi_c)R_b(1 - \cos\varphi_c)\tan\varphi_c + R_b^2(1 - \cos\varphi_c)^2}. \tag{5}$$

The actual deformation of the central stiffener illustrates that the central stiffener exhibits global bending and tension effects when punched by a sphere. However, the stiffener outside the contact region with the indenter is treated as linear in the current study for simplicity to obtain a large deformation resistance. Thus, the global bending effect of the stiffener will concentrate in the plastic hinges (see the dashed area in Figure 3).

The rotation angle of the stiffener γ can be expressed as

$$\tan\gamma = \frac{w_c}{x_c}, \tag{6}$$

where w_c and x_c are the coordinate values at point C, and they can be expressed as

$$\begin{aligned} w_c &= w_{csmax} - R_b + R_b\cos\varphi_c, \\ x_c &= l_s - R_b\sin\varphi_c. \end{aligned} \tag{7}$$

Moreover, w_c and $w_{cs\max}$ are assumed to have the following relation:

$$w_c = c_{cs} w_{cs\max}, \tag{8}$$

where c_{cs} is the ratio of the deflection of point C to the maximum deflection of the central stiffener.

Thus, the relation between the indentation velocities of the point C $\dot{w}_c$ and the central stiffener $\dot{w}_{cs\max}$ can be expressed as

$$\dot{w}_c = c_{cs} \dot{w}_{cs\max}. \tag{9}$$

Then, the angular velocity of rotational stiffener $\dot{\gamma}$ can be obtained:

$$\dot{\gamma} = \frac{\dot{w}_c}{(1 + \tan^2 \gamma) x_c}. \tag{10}$$

The bending energy rate of the central stiffener can be expressed as

$$\dot{E}_{b\_cs} = 4 M_{ps} t_s \dot{\gamma}, \tag{11}$$

where M_{ps} is the plastic bending moment per unit thickness and can be obtained as

$$M_{ps} = \frac{\sigma_{0s} h_s^2}{2}, \tag{12}$$

where σ_{0s} is the flow stress of the stiffener, which is the averaged value of the yield stress σ_{ys} and ultimate tension stress σ_{us} [21].

Moreover, the tension strain ε_{cs} and tension strain rate $\dot{\varepsilon}_{cs}$can be approximated as

$$\begin{aligned} \varepsilon_{cs} &= \frac{1}{2} (\tan \gamma)^2, \\ \dot{\varepsilon}_{cs} &= \tan \gamma \frac{\dot{w}_c}{x_c}. \end{aligned} \tag{13}$$

Thus, the rate of membrane tension of the stiffener can be expressed as

$$\dot{E}_{m\_cs} = 2 \iint_{S_{cs}} \sigma_0 t_s \dot{\varepsilon}_{cs} \mathrm{d}S_{cs}, \tag{14}$$

where S_{cs} is the side of the area on which the central stiffener experiences tension and can be obtained from $S_{cs} = x_c h_s$.

According to the upper bound theorem, the equilibrium equation can be expressed as

$$F_{p\_cs} \dot{w}_{cs\max} = \dot{E}_{b\_cs} + \dot{E}_{m\_cs}, \tag{15}$$

where F_{p_cs} is the resistance of the stiffener in the plastic stage.

Finally, the instantaneous resistance of the stiffener at the plastic stage can be derived by substituting (11) and (14) into (15):

$$F_{p\_cs} = \frac{2 \sigma_{0s} h_s w_c t_s}{(l_s - R_b \sin \varphi_c) w_{cs\max}} \left(\frac{h_s}{1 + \tan^2 \gamma} + w_c \right). \tag{16}$$

2.1.2. Lateral Stiffener. The deformation of the lateral stiffener is driven by the deformed plate. It is assumed that the lateral stiffener deforms simultaneously with the side plate. Thus, the overall movement of the lateral stiffener is the superposition of the lateral deflection from the plate and rotation with the plate. Here, it is assumed that the stiffeners will remain perpendicular to the side plate until plate fracture occurs.

The deformation mode of the stiffener is shown in Figure 4. The ends of the stiffener are welded to adjacent web girders that can constrain the rotation of the stiffener locally. Thus, plastic hinges will be generated at the ends of the stiffeners, which can lead to an out-of-plane bending effect, marked by the red dashed lines in Figure 4. However, the bending effect is neglected because the stiffener out-of-plane bending moment is much smaller than its in-plane bending moment. Therefore, only the membrane tension effect is considered for the lateral stiffener to predict its deformation resistance.

As shown in Figure 4, the deformed stiffener is also placed in the *x*-*w* rectangular coordinate system. The deformation shape of the stiffener can be expressed as

$$w_{ls} = w_{ls\max} \sin\left(\frac{\pi x}{2 l_s} \right), \tag{17}$$

where w_{ls} is the deflection of the stiffener and $w_{ls\max}$ is the maximum transverse deflection of the stiffener.

According to (4), $w_{ls\max}$ can be obtained as

$$\begin{aligned} w_{ls\max} &= w(x_{ls}) = w_{cs\max} \\ &\quad - \sqrt{w_{cs\max}^2 + 2 R_b (\cos \varphi_c - 1) \tan \varphi_c x_{ls}}, \end{aligned} \tag{18}$$

where x_{ls} is the initial horizontal distance between the stiffener and plate edge.

Similar to the relation between w_c and $w_{cs\max}$ for the central stiffener, $w_{ls\max}$ and $w_{cs\max}$ have the following relations:

$$\begin{aligned} w_{ls\max} &= c_{ls} w_{cs\max}, \\ \dot{w}_{ls\max} &= c_{ls} \dot{w}_{cs\max}, \end{aligned} \tag{19}$$

where c_{ls} is the ratio of the maximum deflection between the lateral stiffener and the central stiffener.

As the stiffener is assumed to be displaced vertically, the tension strain ε_{ls} can be approximated as

$$\varepsilon_{ls} \approx \frac{1}{2} \left(\frac{\partial w_{ls}}{\partial x} \right)^2 = w_{ls\max}^2 \frac{\pi^2}{8 l_s^2} \cos^2\left(\frac{\pi x}{2 l_s} \right). \tag{20}$$

The strain rate of the stiffener $\dot{\varepsilon}_{ls}$ can be expressed as

$$\dot{\varepsilon}_{ls} = w_{ls\max} \frac{\pi^2}{4 l_s^2} \cos^2\left(\frac{\pi x}{2 l_s} \right) \dot{w}_{ls\max}. \tag{21}$$

The rate of membrane energy can be expressed as

$$\dot{E}_{m\_ls} = \iint_{S_{ls}} \sigma_{0s} t_s \dot{\varepsilon}_{ls} \mathrm{d}S_{ls}, \tag{22}$$

where S_{ls} is the initial area of the lateral stiffener.

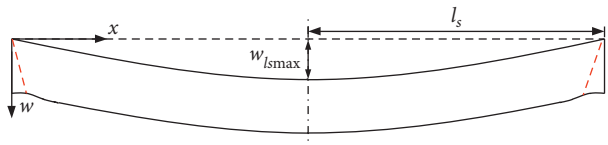

Figure 4: Deformation mode of the lateral stiffener.

According to the upper bound theorem, the rate of work by the external load is equal to the rate of internal energy dissipation. The equilibrium can be expressed as

$$F_{ls} \cdot \dot{w}_{cs\max} = \dot{E}_{m\_ls}. \tag{23}$$

Thus, the instantaneous resistance of the lateral stiffener F_{ls} can be derived as

$$F_{ls} = \frac{\sigma_{0s} t_s h_s \pi^2 w_{ls\max}^2}{4 l_s w_{cs\max}}. \tag{24}$$

2.2. Fracture Prediction of the Stiffened Plate. Analytical fracture prediction for the ship side plate under a bulbous bow striking scenario is crucial for estimating the critical energy dissipation. Several equations were proposed to calculate the critical penetration depth of an unstiffened plate. Recently, an expression that was validated by a number of experiments was proposed by Zhang et al. [15]. This expression is as follows:

$$w_{p\_f} = c_1 \sqrt{(7n + 0.76) b_0 R_b}, \tag{25}$$

where c_1 is the correction coefficient and has been calibrated to be 0.5, n is the work hardening exponent of the plate material, and b_0 is the half-width of the plate.

In particular, the effect of the lateral stiffener on the initial fracture of the ship side plate is considered in this section. An analytical method is proposed to predict the fracture initiation of a stiffened side shell.

Section 2.1.2 demonstrates that the deformation of the lateral stiffener is driven by the plate. Actually, the lateral stiffener interacts with the plate in the large deformation process. Thus, the lateral stiffener is able to restrain the deformation of the plate and finally reduce the critical penetration depth of the plate. Given the critical penetration depth of the plate w_{p_f}, the critical penetration depth for the stiffened plate w_{sp_f} can be expressed as

$$w_{sp\_f} = w_{p\_f} - \mathrm{d}w_{ls}, \tag{26}$$

where $\mathrm{d}w_{ls}$ is the penetration depth reduced by the lateral stiffeners.

The cross section at the maximum deflection of the lateral stiffener is extracted to analyze the influence of the stiffener on the deflection of the plate. Figure 5(a) shows the load state of the plate at the plate-stiffener intersection. At the intersection, angular discontinuity of the curved plate occurs due to the vertical force F_s from the stiffener. The plate also sustains tension from the adjacent plates, which are denoted as F_{p1} and F_{p2}. Figure 5(b) depicts the internal force of the stiffener, where the infinitesimal fragment is $\mathrm{d}s$ in length. According to Section 2.1.2, the stiffener experiences a tension effect, and the tension force F_{Ns} can be expressed as

$$F_{Ns} = \sigma_{0s} t_s h_s. \tag{27}$$

Thus, the vertical force F_s applied by the stiffener can be obtained as

$$F_s = F_{Ns} \frac{\mathrm{d}s}{R_s}, \tag{28}$$

where R_s is the radius of curvature of the deformed stiffener. According to (17), R_s can be obtained as

$$R_s = \frac{\left(1 + \dot{w}_{ls}^2(x)\right)^{3/2}}{\left|\ddot{w}_{ls}(x)\right|}. \tag{29}$$

Moreover, the tension forces from the plate are assumed to be very similar and are expressed as

$$F_{p1} = F_{p2} = \sigma_{0p} t_p \mathrm{d}s, \tag{30}$$

where σ_{0p} is the flow stress of the plate and t_p is the thickness of the plate.

On the y-axis, the resultant force should be zero. Thus, F_s can also be expressed as

$$F_s = F_{p1}(\sin\varphi - \sin(\varphi - \mathrm{d}\varphi)). \tag{31}$$

Considering (28) and substituting (29) and (30) into (31), the increment in the rotation angle at the plate-stiffener intersection can be approximated as

$$\mathrm{d}\varphi = \frac{w_{ls\max} \pi^2 \sigma_{0s} h_s t_s}{4 \sigma_{0p} l_s^2 t_p}. \tag{32}$$

According to (4), the instantaneous angle φ at the plate-stiffener intersection satisfies the following relation:

$$\tan\varphi = \frac{\mathrm{d}w}{\mathrm{d}x} = \frac{R_b(\cos\varphi_c - 1)\tan\varphi_c}{(1 - (1/c_{ls}))w_{ls\max}}. \tag{33}$$

Based on (33), the lateral deflection of the plate limited by the stiffener $\mathrm{d}w_{ls}$ can be approximated as

$$\mathrm{d}w_{ls}(\varphi_c) = \frac{\left(w_{ls\max} - w_p\right) w_{ls\max}}{R_b(\cos\varphi_c - 1)\tan\varphi_c} \mathrm{d}\varphi. \tag{34}$$

Substituting (32) into (34), $\mathrm{d}w_{ls}$ can be further expressed as

$$\mathrm{d}w_{ls}(\varphi_c) = \frac{\sigma_{0s} h_s t_s w_{ls\max}^2 \pi^2 \left(w_{ls\max} - w_{cs\max}\right)}{4 \sigma_{0p} R_b l_s^2 t_p (\cos\varphi_c - 1)\tan\varphi_c}. \tag{35}$$

3. Experimental Details

3.1. Penetration Test Design. The quasistatic indentation experiments were performed at Huazhong University of Science and Technology. The setup used in the experiments is presented in Figure 6(a). The specimens were clamped between a bottom flange and an upper flange, which were made of Q345 steel with a thickness of 25 mm. They were fixed together by M20 bolts. The dimensions of the

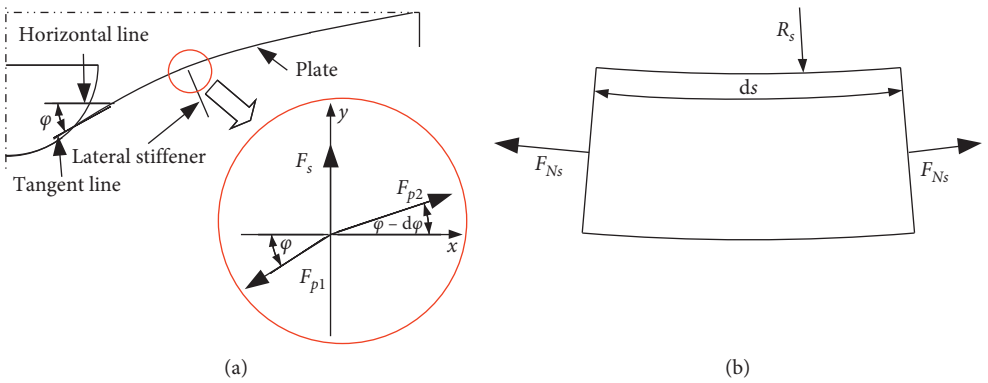

Figure 5: Load state for the components. (a) Plate. (b) Stiffener.

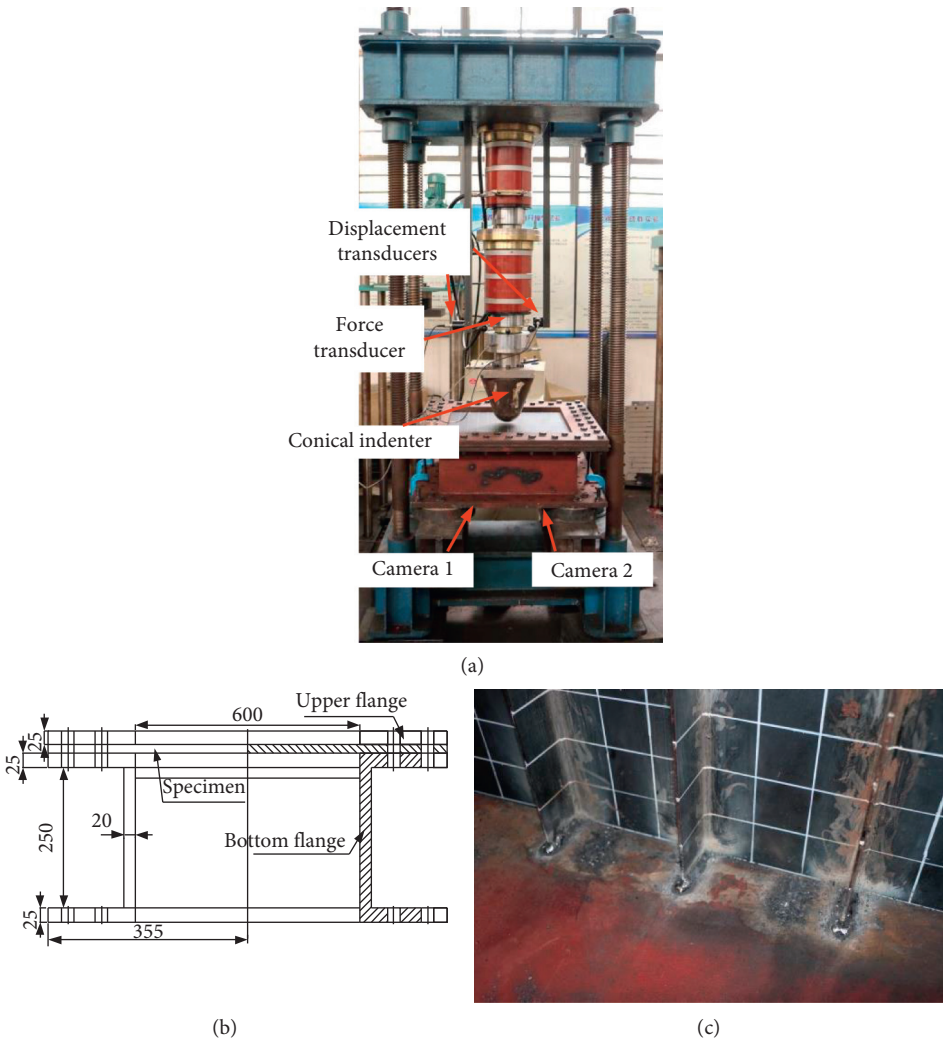

Figure 6: Designed penetration test. (a) Setup. (b) Dimensions of the clamping system. (c) End connections of the stiffeners.

experimental clamping system are illustrated in Figure 6(b). In addition, the ends of the stiffeners were double-side welded on the bottom flange to restrain their freedom, as shown in Figure 6(c). Current fixtures were proven to provide clamped boundary constraints through validation by numerical simulations with solid elements, considering all the fixtures. Moreover, as in previous studies, a bulbous bow is generally treated as rigid and simplified as a conical indenter defined by the top radius [2, 14], as depicted in Figure 2. Thus, the indenter shape was designed to be

conical. The geometry and dimensions are shown in Figure 7.

The initial distance between the indenter and the specimen was approximately 20 mm. The deformation of the specimens was enforced at a rate of ~10 mm/min [2–4] at the midspan by hydraulic cylinders with a 100 ton maximum capacity. A 100-ton load cell fixed between the hydraulic cylinder and the indenter and two displacement sensors jointed on the indenter were utilized to obtain the force-time and displacement-time curves, respectively. To visualize the deformations, 50 × 50 mm grids were drawn on the front and back sides of the specimens. Moreover, two cameras were placed under the bottom flange to capture the deformation process of the specimens.

3.2. Specimens. Three specimens were designed at one-fourth scale from the ship side, as shown in Figure 8. The unstiffened plate (denoted as "US") was used as a reference to estimate the effects of the stiffeners on the resistance and critical penetration depth of the ship side panel. Stiffened plates with two and three stiffeners (denoted as "2FB" and "3FB," respectively) were used to analyze the effects of the lateral stiffener and the central stiffener, respectively. The dimensions of the specimens are also illustrated in Figure 8, where the central 600 × 600 mm square is the exposed area of the panels and the surrounding areas with a width of 155 mm are clamped to the specimens. In addition, all the stiffeners were 55 mm in height. The weld joint plate-stiffeners are alternatively double-sided filled welds with a size of ~3.0 mm. The selected electrodes were ASME (American Society of Mechanical Engineers) ER70S-6 with a diameter of 0.8 mm. The selection of the weld size and the electrode base material follows standard shipyard welding procedures. Moreover, the finished specimens were hammered at the plate-stiffener intersections by a mallet to release the residual stress. Furthermore, replicate tests for each specimen were performed to ensure the reliability of the experimental results.

The material used for the plates and stiffeners is grade B normal structural steel qualified by the CCS (China Classification Society), considering the availability of the thin steel plate and the loading capacity of the hydraulic cylinder. These steel plates were from the same batch supplied by WISCO (Wuhan Iron and Steel (Group) Company) and were all 3.15 mm thick. To obtain the mechanical properties of the steel, quasistatic tensile tests are conducted using three standard tensile specimens and procedures. The dimensions of the machined tension test pieces are shown in Figure 9. Based on the displacement-prescribed tensile tests performed on the universal testing machine, the engineering stress-strain behavior of the material can be obtained. The tensile engineering stress-strain curve is presented in Figure 10. The mechanical properties of the plate material are summarized in Table 1, where n is obtained according to Ref. [15].

3.3. Results. The experimentally measured resistance-penetration curves are shown in Figure 11. In addition, the deformation shapes when the plates are initially fractured are shown in Figure 12 for the three specimens. These curves

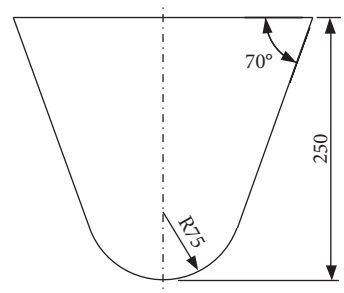

Figure 7: Dimensions of the conical indenter (dimensions in mm).

demonstrate that the lateral stiffener and the central stiffener can both supply an extent of lateral resistance at different penetration depths compared with the unstiffened plate. In addition, the improved resistances due to the lateral and central stiffeners are close at different penetration depths. The resistance improved by the central stiffener is more remarkable than that by the lateral stiffener. In addition, the resistance-penetration curves indicate that the critical penetration depths for the three specimens are different. Compared with specimen US, the reductions in the critical penetration depth of specimen 2FB and specimen 3FB are 9.1 mm and 7.8 mm, respectively. This value for specimen 2FB is larger because the horizontal distance between the lateral stiffener and the impact position is smaller, which can lead to a stronger restriction effect in the plate.

Moreover, the influence of stiffener tripping on the lateral deformation resistance is evaluated. Figure 13 shows the experimental observations when fractures are initially generated in the side plate. The central stiffener in specimen 3FB remains upright, while the central stiffener in the replicate test trips down. Current experiments illustrate that the tripping extent of the stiffeners can vary greatly due to the differences in the welding conditions and the relative specimen-indenter impact locations. In addition, the corresponding resistance-penetration responses for these two specimens are shown in Figure 13. The compared curves demonstrate that the discrepancy of the resistance-penetration responses is small in the experiments, which proves that the tripping of the central stiffener has a slight influence on the resistance response. Clearly, this conclusion is different from that stated by Yu et al. [20]. The reason for this difference is attributed to the variations in the structural forms of the central stiffener in these two studies. The investigated stiffener in Yu et al. [20] is the T-profile stiffener, where the top flange will experience a remarkable membrane tension effect. Tripping of the T-profile stiffener can reduce the lateral deflection of the top flange, thereby leading to a significant decrease in resistance. Meanwhile, tripping of the stiffener's web will have little influence on the lateral resistance of the stiffened plate.

4. Verification of the Analytical Prediction Method

In this section, the proposed analytical method is verified with respect to the large deformation resistance and the

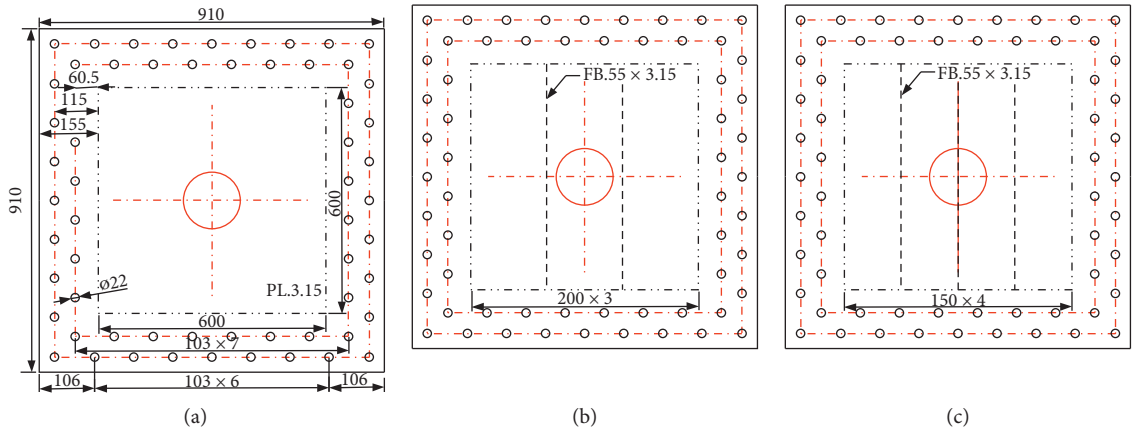

Figure 8: Dimensions of the specimens (dimensions in mm). (a) Specimen US. (b) Specimen 2FB. (c) Specimen 3FB.

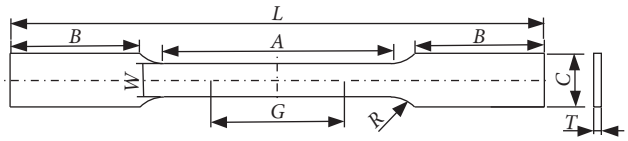

G-Gauge length	50 mm
W-Width	12.5 mm
T-Thickness	3.15 mm
R-Radius of fillet	12.5 mm
L-Overall length	200 mm
A-Length of reduced section	85 mm
B-Length of grip section	~50 mm
C-Width of grip section	20 mm

Figure 9: Dimensions of the standard tension tested piece (ASTM, E8). G, gauge length (50 mm); W, width (12.5 mm); T, thickness (3.15 mm); R, radius of fillet (3.15 mm); L, overall length (200 mm); A, length of reduced section (85 mm); B, length of grid section (~50 mm); C, width of grip section (20 mm).

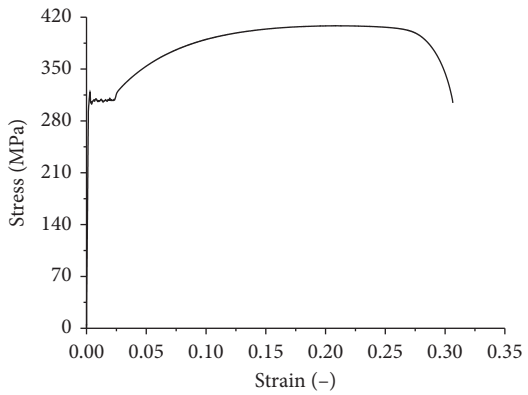

Figure 10: Engineering stress-strain curve.

critical penetration depth of the stiffened plate by comparing the analytically predicted resistance-penetration curves with the experimental curves, as shown in Figure 14. Moreover, the workflow for obtaining the resistance-penetration relation for the stiffened plate is given in Figure 15.

Table 1: Mechanical properties of material.

Property	Symbol	Units	Specimens
Young's modulus	E	GPa	207
Poisson's ratio	ν	—	0.3
Mass density	ρ	kg/m^3	7850
Yield stress	σ_Y	MPa	302.8
Ultimate tensile strength	σ_u	MPa	408.4
Fracture strain	ε_f	—	0.306
Strain-hardening index	n	—	0.2

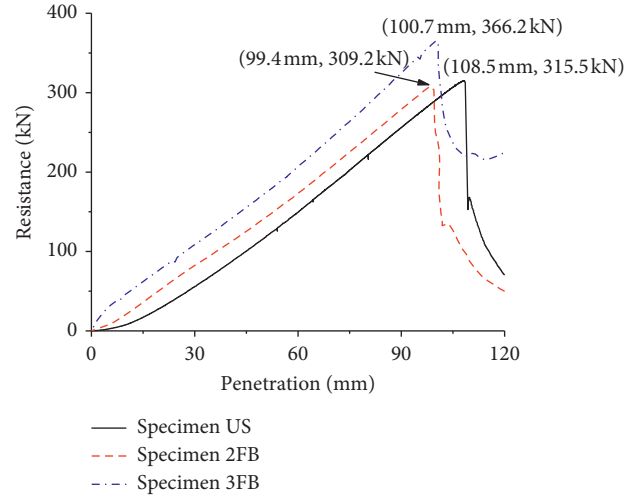

Figure 11: Experimental resistance-penetration responses.

The current study proposes not only analytical predictions for the deformation resistance of the central stiffener and the lateral stiffener but also a method to obtain the critical penetration depth of the stiffened plate. With the analytical solutions for the large deformation resistance and the critical penetration depth of the unstiffened plate in Ref. [15], the analytical predictions for a stiffened plate can be obtained from large deformation to initial fracture. The compared resistance-penetration curves shown in Figure 14 illustrate that the analytical method can adequately predict

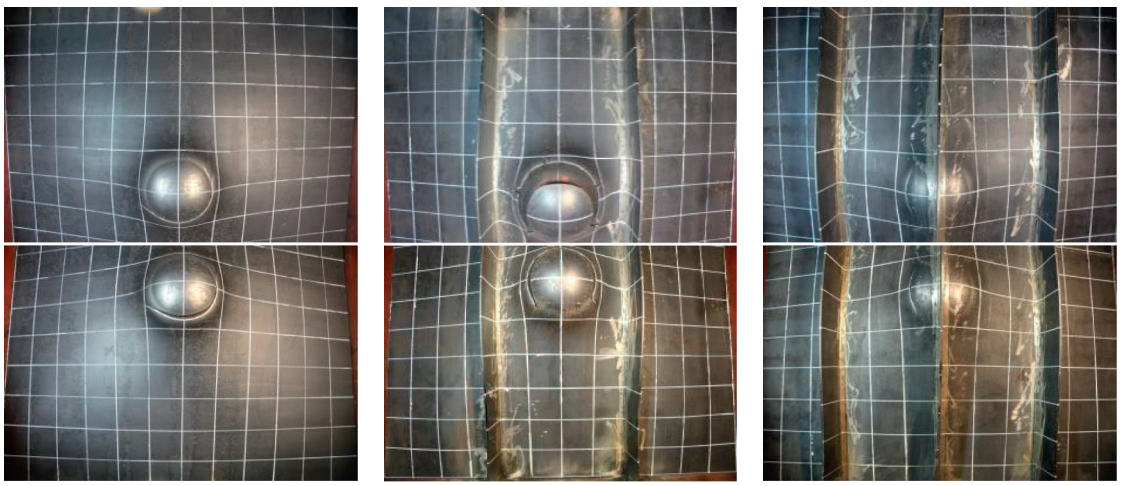

(a) (b) (c)

Figure 12: Deformation shapes of specimens when plates are initially fractured. (a) Specimen US. (b) Specimen 2FB. (c) Specimen 3FB.

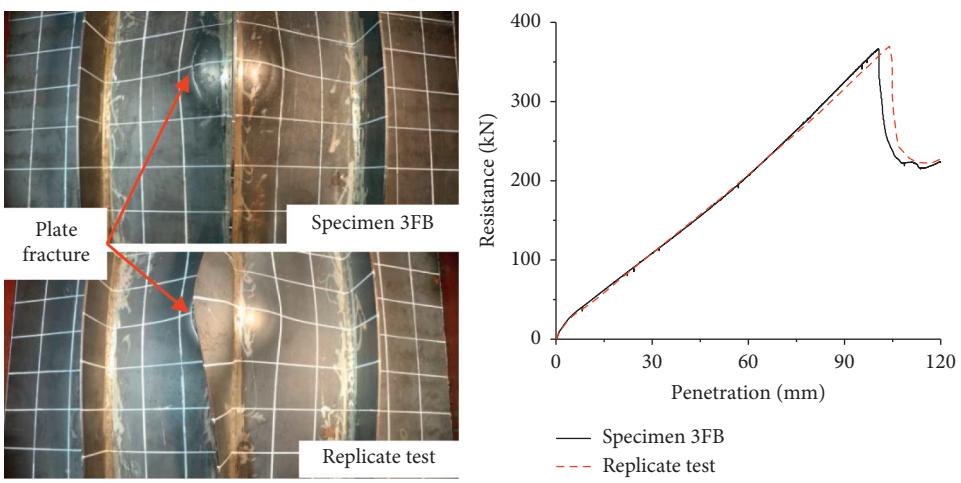

Figure 13: Experimental results for specimen 3FB and the replicate test.

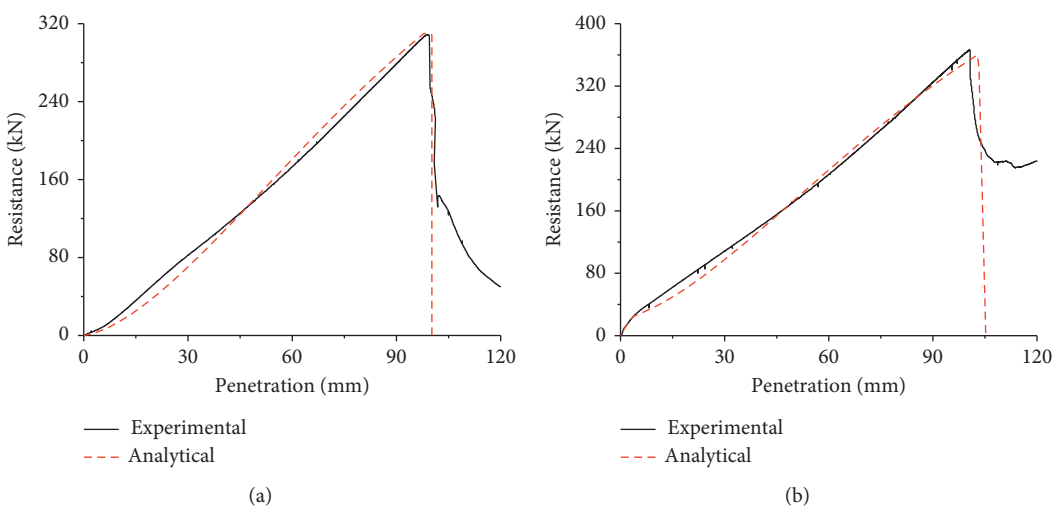

Figure 14: Comparison of analytical and experimental resistance-penetration responses. (a) Specimen 2FB. (b) Specimen 3FB.

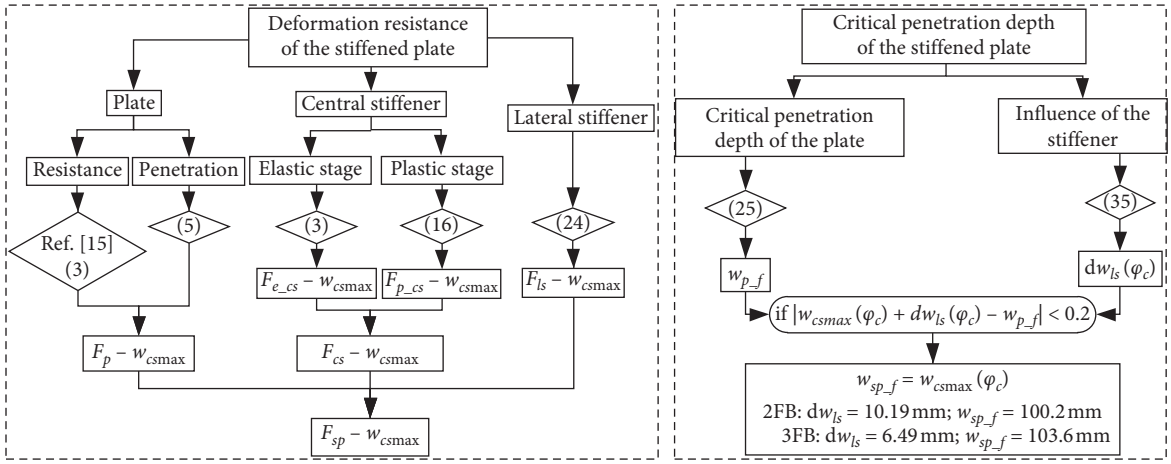

Figure 15: Calculation of the resistance-penetration relation for the stiffened plate.

the resistance due to the large deformation and fracture initiation of the stiffened plate. This demonstrates that the proposed analytical method can accurately estimate the crashworthiness of a ship side plate impacted by a bulbous bow.

In particular, the current study considers the influence of the stiffener on the critical penetration depth of the plate. Thus, the solution of the critical penetration depth for the stiffened plate is described in detail. First, the critical penetration depth for the plate can be calculated according to (25). Then, the penetration depth reduced by the lateral stiffener is calculated based on (35). Finally, the critical penetration depth of the stiffened plate can be determined when satisfying the equation in Figure 15. According to the similarity of the resistance-penetration curves, the proposed analytical method can predict the initial fracture of the stiffened plate with flat-bar stiffeners.

5. Conclusions

This paper assesses the effects of stiffeners on the crashworthiness of the ship side shell impacted by a bulbous bow. Analytical expressions are presented to calculate the large deformation resistances for the lateral and central flat-bar stiffeners and the critical penetration depth for the stiffened plate. The deformation shape of the central stiffener is identical to that of the plate. However, the deformation mode of the central stiffener outside the contact region with the indenter is treated as linear for simplicity to calculate the deformation resistance. In addition, the deformation mode of the lateral stiffener is treated as a sine curve to obtain its deformation resistance and the reduction in the critical penetration depth of the plate due to the tension effect.

Model tests with three specimens (one unstiffened plate for reference and two stiffened plates) quasistatically punched by a conical indenter are performed. The resistance-penetration curves and the damage shapes are obtained through the experiments. The experimental results illustrate that the improvement in resistance due to the central stiffener is more remarkable than that of the lateral stiffener. In addition, a smaller distance between the lateral stiffener and the indentation position can lead to a lower critical penetration depth of the ship side panel. Moreover, the resistance response influenced by the tripping of the stiffener web is small. Furthermore, the similarity of the experimental and analytical resistance-penetration curves demonstrates the reliability and accuracy of the proposed simplified analytical method.

Nomenclature

b_0: Half-width of the rectangular plate
dw_{ls}: Penetration depth reduced by the lateral stiffener
E: Elastic modulus
F_{e_cs}: Elastic resistance of the central stiffener
F_{ls}: Resistance of the lateral stiffener
F_p: Resistance of the unstiffened plate
F_{p_cs}: Plastic resistance of the central stiffener
F_{sp}: Resistance of the stiffened plate
h_s: Stiffener height
l_s: Half-length of the stiffener
n: Work hardening exponent of the plate material
R_b: Radius of the spherical punch
t_p: Plate thickness
t_s: Stiffener thickness
w_c: Vertical distance from the point C to initial shape
$w_{cs\,max}$: Maximum deflection of the central stiffener
w_{ls}: Deflection of the lateral stiffener
$w_{ls\,max}$: Maximum transverse deflection of the lateral stiffener
w_{p_f}: Critical penetration depth of the plate
w_{sp_f}: Critical penetration depth of the stiffened plate
φ_c: Indenter wrapping angle at the outermost contact point
γ: Rotation angle of the central stiffener
ε_{cs}: Tension strain of the central stiffener
ε_{ls}: Tension strain of the lateral stiffener
x_c: Horizontal distance from the point C to plate edge
x_{ls}: Initial horizontal distance between the stiffener and plate edge
σ_{0p}: Flow stress of the plate
σ_{0s}: Flow stress of the stiffener.

Data Availability

The data used to support the findings of this study are available from the corresponding author upon request.

Conflicts of Interest

The authors declare that they have no conflicts of interest.

Acknowledgments

This study was supported by the Foundation of Wuhan Polytechnic University (grant no. 2020Y09) and National Natural Science Foundation of China (grant no. 51579110).

References

[1] L. Hong, *Simplifed analysis and design of ships subjected to collision and grounding*, Ph.D. thesis, Norwegian University of Science and Technology, Trondheim, Norway, 2009.

[2] H. S. Alsos and J. Amdahl, "On the resistance to penetration of stiffened plates, part I—experiments," *International Journal of Impact Engineering*, vol. 36, no. 6, pp. 799–807, 2009.

[3] D. Morin, B. L. Kaarstad, B. Skajaa, O. S. Hopperstad, and M. Langseth, "Testing and modelling of stiffened aluminium panels subjected to quasi-static and low-velocity impact loading," *International Journal of Impact Engineering*, vol. 110, pp. 97–111, 2017.

[4] M. Kõrgesaar, J. Romanoff, H. Remes, and P. Palokangas, "Experimental and numerical penetration response of laser-welded stiffened panels," *International Journal of Impact Engineering*, vol. 114, pp. 78–92, 2018.

[5] L. Yang and D.-Y. Wang, "Experimental and numerical investigation on the response of stiffened panels subjected to lateral impact considering material failure criteria," *Ocean Engineering*, vol. 184, pp. 193–205, 2019.

[6] M. A. G. Calle and M. Alves, "A review-analysis on material failure modeling in ship collision," *Ocean Engineering*, vol. 106, pp. 20–38, 2015.

[7] M. Kõrgesaar, "The effect of low stress triaxialities and deformation paths on ductile fracture simulations of large shell structures," *Marine Structures*, vol. 63, pp. 45–64, 2019.

[8] B. C. Cerik, K. Lee, S.-J. Park, and J. Choung, "Simulation of ship collision and grounding damage using Hosford-Coulomb fracture model for shell elements," *Ocean Engineering*, vol. 173, pp. 415–432, 2019.

[9] H. Zhiqiang, A. Jørgen, and H. Lin, "Verification of a simplified analytical method for predictions of ship groundings over large contact surfaces by numerical simulations," *Marine Structures*, vol. 24, no. 4, pp. 436–458, 2011.

[10] N. Jones, *Structual Impact*, Cambridge University Press, Cambridge, UK, 2nd edition, 2012.

[11] B. Liu, "Analytical method to assess double-hull ship structures subjected to bulbous bow collision," *Ocean Engineering*, vol. 142, pp. 27–38, 2017.

[12] B. C. Simonsen and L. P. Lauridsen, "Energy absorption and ductile failure in metal sheets under lateral indentation by a sphere," *International Journal of Impact Engineering*, vol. 24, no. 10, pp. 1017–1039, 2000.

[13] Y.-W. Lee, J. C. Woertz, and T. Wierzbicki, "Fracture prediction of thin plates under hemi-spherical punch with calibration and experimental verification," *International Journal of Mechanical Sciences*, vol. 46, no. 5, pp. 751–781, 2004.

[14] Y. Gong, Y. Gao, D. Xie, and J. Liu, "Deflection and fracture of a clamped plate under lateral indentation by a sphereflection and fracture of a clamped plate under lateral indentation by a sphere," *Ocean Engineering*, vol. 103, pp. 21–30, 2015.

[15] M. Zhang, Q. Sun, J. Liu, Z. Hu, and S. Zhang, "A study of the rupture behavior of a ship side plate laterally punched by a full-shape bulbous bow indenter," *Ocean Engineering*, vol. 182, pp. 48–60, 2019.

[16] S.-R. Cho and H.-S. Lee, "Experimental and analytical investigations on the response of stiffened plates subjected to lateral collisions," *Marine Structures*, vol. 22, no. 1, pp. 84–95, 2009.

[17] B. Liu, R. Villavicencio, and C. Guedes Soares, "Simplified analytical method to evaluate tanker side panels during minor collision incidents," *International Journal of Impact Engineering*, vol. 78, pp. 20–33, 2015.

[18] B. Sun, Z. Hu, and G. Wang, "An analytical method for predicting the ship side structure response in raked bow collisions," *Marine Structures*, vol. 41, pp. 288–311, 2015.

[19] M. Zhang, J. Liu, Z. Hu, and Y. Zhao, "On resistance of a rectangular thin plate under lateral indentation by a wedge indenter," *Ships and Offshore Structures*, vol. 13, no. 6, pp. 617–629, 2018.

[20] Z. Yu, J. Amdahl, and Y. Sha, "Large inelastic deformation resistance of stiffened panels subjected to lateral loading," *Marine Structures*, vol. 59, pp. 342–367, 2018.

[21] Z. G. Gao, S. Yang, and Z. Q. Hu, "The resistance of ship web girders in collision and grounding," *Mathematical Problems in Engineering*, vol. 2014, Article ID 720542, 13 pages, 2014.